Monthly Notices
of the
ROYAL ASTRONOMICAL SOCIETY

Mon. Not. R. Astron. Soc. **420,** 483–494 (2012) doi:10.1111/j.1365-2966.2011.20053.x

Gamma-ray bursts in the comoving frame

G. Ghirlanda,[1⋆] L. Nava,[2] G. Ghisellini,[1] A. Celotti,[2] D. Burlon,[3] S. Covino[1] and A. Melandri[1]

[1]*INAF – Osservatorio Astronomico di Brera, Via E. Bianchi 46, I-23807 Merate, Italy*
[2]*SISSA – via Bonomea, 265, I-34136 Trieste, Italy*
[3]*Max Planck Institut für Extraterrestrische Physik, Giessenbachstraße 1, D-85478 Garching, Germany*

Accepted 2011 October 21. Received 2011 October 3; in original form 2011 July 20

ABSTRACT

We estimate the bulk Lorentz factor Γ_0 of 31 gamma-ray bursts (GRBs) using the measured peak time of their afterglow light curves. We consider two possible scenarios for the estimate of Γ_0: the case of a homogeneous circumburst medium or a wind density profile. The values of Γ_0 are broadly distributed between few tens and several hundreds with average values $\sim$138 and $\sim$66 for the homogeneous and wind density profile, respectively. We find that the isotropic energy and luminosity correlate in a similar way with Γ_0, i.e. $E_{\rm iso} \propto \Gamma_0^2$ and $L_{\rm iso} \propto \Gamma_0^2$, while the peak energy $E_{\rm peak} \propto \Gamma_0$. These correlations are less scattered in the wind density profile than in the homogeneous case. We then study the energetics, luminosities and spectral properties of our bursts in their comoving frame. The distribution of $L'_{\rm iso}$ is very narrow with a dispersion of less than a decade in the wind case, clustering around $L'_{\rm iso} \sim 5 \times 10^{48}$ erg s^{-1}. Peak photon energies cluster around $E'_{\rm peak} \sim 6$ keV. The newly found correlations involving Γ_0 offer a general interpretation scheme for the spectral energy correlation of GRBs. The $E_{\rm peak}$–$E_{\rm iso}$ and $E_{\rm peak}$–$L_{\rm iso}$ correlations are due to the different Γ_0 factors and the collimation-corrected correlation, $E_{\rm peak}$–E_γ (obtained by correcting the isotropic quantities for the jet opening angle $\theta_{\rm j}$), can be explained if $\theta_{\rm j}^2\Gamma_0 =$ constant. Assuming the $E_{\rm peak}$–E_γ correlation as valid, we find a typical value of $\theta_{\rm j}\Gamma_0 \sim$ 6–20, in agreement with the predictions of magnetically accelerated jet models.

Key words: radiation mechanisms: non-thermal – gamma-ray burst: general.

1 INTRODUCTION

The discovery of the afterglows of gamma-ray bursts (GRBs; Costa et al. 1997) allowed to pinpoint their position in the X-ray and optical bands. This opened a new era focused at measuring the spectroscopic redshifts of these sources. The present[1] collection of GRBs with measured z consists of 232 events. In 132 bursts of this sample (updated in this paper), the peak energy $E_{\rm peak}^{\rm obs}$ of their νF_ν prompt emission γ-ray spectrum could be constrained. In turn, for these bursts it was possible to calculate the isotropic equivalent energy $E_{\rm iso}$ and luminosity $L_{\rm iso}$. The knowledge of the redshifts showed that two strong correlations exist between the *rest frame* peak energy $E_{\rm peak}$ and $E_{\rm iso}$ or $L_{\rm iso}$ (also known as the 'Amati' and 'Yonetoku' correlations – Amati et al. 2002; Yonetoku et al. 2004, respectively).

The reality of these correlations has been widely discussed in the literature. Some authors pointed out that they can be the result of observational selection effects (Band & Preece 2005; Nakar & Piran 2005; Butler et al. 2007; Butler, Kocevski & Bloom 2009; Shahmoradi & Nemiroff 2011) but counter-arguments have be en put forward arguing that selection effects, even if surely present, play a marginal role (Ghirlanda et al. 2005, 2008; Bosnjak et al. 2008; Nava et al., 2008; Amati, Frontera & Guidorzi 2009; Krimm et al. 2009). The finding that a correlation $E_{\rm p}(t)$–$L_{\rm iso}(t)$ exists when studying time-resolved spectra of individual bursts is a strong argument in favour of the reality of the spectral energy correlations, (Ghirlanda, Nava & Ghisellini 2010b; Ghirlanda et al. 2011) and motivates the search for the underlying process generating them. Even if several ideas have been already discussed in the literature, there is no general consensus yet, and a step forward towards a better understanding both of the spectral energy correlations and the underlying radiation process of the prompt emission of GRBs is to discover what are the typical energetics, peak frequencies and peak luminosities in the *comoving frame*.

The physical model of GRBs requires that the plasma emitting γ-rays should be moving relativistically with a bulk Lorentz factor Γ_0 much larger than unity. The high photon densities and the short time-scale variability of the prompt emission imply that GRBs are

⋆E-mail: giancarlo.ghirlanda@brera.inaf.it
[1] http://www.mpe.mpg.de/jcg/grbgen.html

optically thick to pair production which, in turn, would lead to a strong suppression of the emitted flux, contrary to what observed. The solution of this compactness problem requires that GRBs are relativistic sources. From this argument lower limits $\Gamma_0 \geq 100$ are usually derived (Lithwick & Sari 2001). The first observational evidences supporting this scenario were found in the radio band where the ceasing of the radio flux scintillation (few weeks after the explosion as in GRB 970508; Frail et al. 1997), allowed to estimate Γ of a few. This value corresponds to the late afterglow phase, when the fireball is decelerated almost completely by the interstellar medium (ISM) and is characterized by a much smaller bulk Lorentz factor than the typical Γ_0 of the prompt phase.

Large Lorentz factors imply strong beaming of the radiation we see. We are used to consider GRB intrinsic properties ($E_{\rm peak}$, $E_{\rm iso}$, $L_{\rm iso}$) for the bursts with measured redshifts, but still an important correction should be applied. Our aim is to study the distributions of $E_{\rm peak}$, $E_{\rm iso}$, $L_{\rm iso}$ and the spectral energy correlations ($E_{\rm peak}$–$E_{\rm iso}$ and $E_{\rm peak}$–$L_{\rm iso}$) in the *comoving frame*, accounting for the Γ_0 factor. The estimate of Γ_0 is possible by measuring the peak of the afterglow (Sari & Piran 1999) and has been successfully applied in some cases (e.g. Molinari et al. 2007, Gruber et al. 2011) and more extensively recently by Liang, Yi & Zhang (2010) in the optical and X-ray band. Other methods allow us to set lower limits (Abdo et al. 2009a,b; Ackermann et al. 2010) mainly by applying the compactness argument to the high-energy emission recently detected in few GRBs at GeV energies by the *Fermi* satellite (see Hascoet et al. 2011; Zhao, Li & Bai 2011; Zou, Fan & Piran 2011, for more updated calculation on these lower limits on Γ_0). Conversely, upper limits (Zou & Piran 2010) can be derived by requiring that the forward shock emission of the afterglow does not appear in the MeV energy band.

The paper is organized as follows. In Section 2 we discuss the relativistic corrections that allow us to derive the comoving frame $E'_{\rm peak}$, $E'_{\rm iso}$ and $L'_{\rm iso}$ from the rest frame $E_{\rm peak}$, $E_{\rm iso}$, $L_{\rm iso}$. In Sections 3 and 4 we derive a general formula for the estimate of Γ_0 from the measurement of the time of the peak of the afterglow emission. In Section 5 we present our sample of GRBs and in Section 6 our results, which are finally discussed in Section 7. Throughout the paper we assume a standard cosmology with $h = \Omega_\Lambda = 0.7$ and $\Omega_{\rm m} = 0.3$.

2 FROM THE REST TO THE COMOVING FRAME

In this section we derive the Lorentz transformations to pass from rest frame quantities to the same quantities in the comoving frame. This is not trivial, since, differently from the analogue case of blazars, the emitting region is not a blob with a mono-directional velocity, but a fireball with a radial distribution of velocities. Therefore, an observer located on axis receives photons from a range of viewing angles, complicating the transformations from rest frame to comoving quantities. We are interested to three observables: the peak energy $E_{\rm peak}$, the isotropic equivalent energy $E_{\rm iso}$ and the isotropic equivalent peak luminosity $L_{\rm iso}$. Dealing with isotropic equivalent quantities, we can assume that the emitting region is a spherical shell with velocities directed radially. We also assume that the comoving frame bolometric intensity I' is isotropic. We then adopt the usual relation between observed (I) and comoving (I') bolometric intensity:

$$I = \delta^4 I'; \qquad \delta = \frac{1}{\Gamma(1-\beta\cos\theta)}, \tag{1}$$

where δ is the Doppler factor and θ is the angle between the velocity vector and the line of sight. The received flux is

$$F = 2\pi I' \int_0^\pi \delta^4 \sin\theta {\rm d}\theta. \tag{2}$$

Since the fluence $\mathcal{F}$ is a time-integrated quantity, we have $\mathcal{F} \propto \int_0^\pi \delta^3 \sin\theta {\rm d}\theta$, i.e. one power of δ less.

$E_{\rm peak}$: this quantity can be derived from the time-integrated spectrum, or can be the spectral peak energy of a given time interval. In this paper we will use the time-integrated $E_{\rm peak} = E^{\rm obs}_{\rm peak}(1+z)$. The received fluence ${\rm d}\mathcal{F}/{\rm d}\theta$ (i.e. the flux integrated in time) from each annulus of same viewing angle θ is ${\rm d}\mathcal{F}/{\rm d}\theta \propto \sin\theta\delta^3$. For $\theta \to 0$ the Doppler factor is maximum, but the solid angle vanishes, while for $\theta > 1/\Gamma$ the solid angle is large, but δ is small. Therefore, there will be a specific angle θ for which ${\rm d}\mathcal{F}/{\rm d}\theta$ is maximum. This is given by

$$\cos\theta = \beta + \frac{2}{5\Gamma^2}. \tag{3}$$

At this angle the beaming factor is

$$\delta = \frac{5}{3}\Gamma. \tag{4}$$

We then set $E'_{\rm peak} = E_{\rm peak}/(5\Gamma/3)$.

$E_{\rm iso}$: this is proportional to the fluence $\mathcal{F}$, and the relation between the observed and comoving quantity is

$$\frac{E_{\rm iso}}{E'_{\rm iso}} = \frac{\mathcal{F}}{\mathcal{F}'} = \frac{\int_0^\pi \delta^3 \sin\theta {\rm d}\theta}{\int_0^\pi \sin\theta {\rm d}\theta} = \Gamma. \tag{5}$$

We then set $E'_{\rm iso} = E_{\rm iso}/\Gamma$.

$L_{\rm iso}$: this is proportional to the flux F, so the ratio $L_{\rm iso}/L'_{\rm iso}$ is

$$\frac{L_{\rm iso}}{L'_{\rm iso}} = \frac{F}{F'} = \frac{\int_0^\pi \delta^4 \sin\theta {\rm d}\theta}{\int_0^\pi \sin\theta {\rm d}\theta} \sim \frac{4}{3}\Gamma^2. \tag{6}$$

We then set $L'_{\rm iso} = L_{\rm iso}/(4\Gamma^2/3)$ (in agreement with Wijers & Galama 1999).

3 ESTIMATE OF THE BULK LORENTZ FACTOR Γ_0

In the thin-shell regime (i.e. for $T_{90} < t_{\rm peak,obs}$, condition satisfied for almost all bursts in our sample), the standard afterglow theory predicts that the peak of the bolometric afterglow light curve corresponds to the start of the fireball deceleration. The deceleration radius is commonly defined as the radius at which the swept-up matter $m(r_{\rm dec})$ is smaller by a factor Γ_0 than the initial shell's rest mass $M_0 = E_0/(\Gamma_0 c^2)$. Usually, the deceleration time $t_{\rm dec}$ is estimated as $t_{\rm dec} = r_{\rm dec}/(2c\Gamma_0^2)$ (Sari & Piran 1999). This relation is approximate, since it does not consider that the Lorentz factor is decreasing. Some authors consider this relation to estimate Γ_0 from the peak time of the afterglow light curve (Sari 1997; Sari & Piran 1999), while other authors consider that $t_{\rm dec} = r_{\rm dec}/(2c\Gamma^2_{\rm dec})$, where approximately $\Gamma_0 \simeq 2\Gamma(r_{\rm dec})$ (Molinari et al. 2007).

We propose here a detailed and general calculation of Γ_0 which extends the estimate to the generic case of a circumburst density profile described by $n = n_0 r^{-s}$. We use the shape of the light curve in two different power-law regimes: the coasting phase when $r \ll r_{\rm dec}$ and $\Gamma(r) = \Gamma_0$, and the deceleration phase when $r_{\rm dec} \ll r \ll r_{\rm NR}$ (where $r_{\rm NR}$ marks the start of the non-relativistic regime). During the deceleration regime, the evolution of the Lorentz factor is described by the self-similar solution found by Blandford & McKee (1976):

$$\Gamma = \sqrt{\frac{(17-4s)E_0}{(12-4s)m(r)c^2}}. \tag{7}$$

The relation between the radius and the observed time is obtained by integrating the differential equation $\mathrm{d}r = 2c\Gamma^2(r)\mathrm{d}t$ and by considering the exact evolution of Γ with r. From equation (6),

$$L_{\rm iso} = \frac{4}{3}\Gamma^2 L'_{\rm iso} = \varepsilon_{\rm e}\frac{4}{3}\Gamma^2\frac{\mathrm{d}E'_{\rm diss}}{\mathrm{d}t'}, \tag{8}$$

where the dissipated comoving energy $E'_{\rm diss}$ is given by (Panaitescu & Kumar 2000)

$$E'_{\rm diss} = (\Gamma - 1)m(r)c^2. \tag{9}$$

Only a fraction $\varepsilon_{\rm e}$ of the dissipated energy is radiated. We assume that this quantity is small and does not affect the dynamics of the fireball (adiabatic regime). Equation (8) holds until the emission process is efficient (fast-cooling regime).

During the coasting phase $\Gamma = \Gamma_0 \gg 1$ and the luminosity (denoted by $L_{\rm iso,1}$) is

$$L_{\rm iso,1} = \varepsilon_{\rm e}\frac{4}{3}\Gamma_0^3 c^2\frac{\mathrm{d}m(r)}{\mathrm{d}t'} = \varepsilon_{\rm e}\frac{4}{3}\Gamma_0^4 c^3 4\pi r^{(2-s)} n_0 m_{\rm p}. \tag{10}$$

Since in this phase the Lorentz factor is constant and equal to Γ_0, the relation between the fireball radius and the observed time is

$$r = 2ct\Gamma_0^2.$$

As a function of time, the luminosity is

$$L_{\rm iso,1} = \varepsilon_{\rm e}\frac{4}{3}2^{(4-s)}\pi n_0 m_{\rm p} c^{(5-s)}\Gamma_0^{8-2s} t^{2-s}. \tag{11}$$

For a homogeneous density medium ($s = 0$) the light curve rises as t^2. The luminosity is instead constant when $s = 2$, which corresponds to the stellar wind density profile.

To derive the luminosity during the deceleration phase we start again from equations (8) and (9). However, in this case Γ is decreasing according to equation (7) (but still $\Gamma \gg 1$). We derive

$$L_{\rm iso,2} = \varepsilon_{\rm e}\frac{4}{3}\Gamma^2 c^2\left[\Gamma\frac{\mathrm{d}m(r)}{\mathrm{d}t'} + m(r)\frac{\mathrm{d}\Gamma}{\mathrm{d}t'}\right]. \tag{12}$$

The first term of the sum in square brackets can be written as

$$\Gamma\frac{\mathrm{d}m(r)}{\mathrm{d}r}\frac{\mathrm{d}r}{\mathrm{d}t'} = (3-s)\frac{m(r)}{r}\Gamma^2 c.$$

The second term of the sum becomes

$$m(r)\frac{\mathrm{d}\Gamma}{\mathrm{d}r}\frac{\mathrm{d}r}{\mathrm{d}t'} = -\frac{3-s}{2}\frac{m(r)}{r}\Gamma^2 c.$$

During the deceleration,

$$t = \frac{1}{2c}\int\frac{\mathrm{d}r}{\Gamma^2} = \frac{r}{2(4-s)c\Gamma^2},$$

where we have used $\Gamma(r)$ given in equation (7).

For $\Gamma_0 \gg 1$ the initial energy content of the fireball $E_0 = E_{\rm k,iso} + M_0c^2 \simeq E_{\rm k,iso}$, where $E_{\rm k,iso}$ is the isotropic kinetic energy powering the expansion of the fireball in the ISM during the afterglow phase. If the radiative efficiency η of the prompt phase is small, $E_{\rm k,iso}$ can be estimated from the energetics of the prompt as $E_{\rm k,iso} = E_{\rm iso}/\eta$. We obtain

$$\begin{aligned} L_{\rm iso,2} &= \varepsilon_{\rm e}\frac{4}{3}\Gamma^2 c^2\frac{(3-s)m(r)}{4(4-s)t} \\ &= \varepsilon_{\rm e}\frac{4}{3}\frac{(17-4s)(3-s)E_{\rm iso}}{4(12-4s)(4-s)\eta}t^{-1}. \end{aligned} \tag{13}$$

The peak time of the light curve is the time when the coasting phase ends and the deceleration phase starts and can be estimated by setting $L_{\rm iso,1}(t_{\rm peak}) = L_{\rm iso,2}(t_{\rm peak})$:

$$t_{\rm peak} = \left[\frac{(17-4s)(3-s)E_{\rm iso}}{2^{6-s}\pi n_0 m_{\rm p} c^{5-s}\eta(12-4s)(4-s)\Gamma_0^{8-2s}}\right]^{1/(3-s)}, \tag{14}$$

and inverting this relation to obtain the initial Lorentz factor as a function of the peak time:

$$\Gamma_0 = \left[\frac{(17-4s)(3-s)E_{\rm iso}}{2^{6-s}\pi n_0 m_{\rm p} c^{5-s}\eta(12-4s)(4-s)t_{\rm peak}^{3-s}}\right]^{1/(8-2s)}, \tag{15}$$

where $t_{\rm peak}$ is the peak of the afterglow light curve in the source rest frame, i.e. $t_{\rm peak} = t_{\rm peak,obs}/(1+z)$, and it will be indicated as $t_{\rm p,z}$ hereafter.

While a wind density profile (hereafter W: wind ISM) is expected from a massive star progenitor that undergoes strong wind mass losses during the final stages of its life (Chevalier & Li 1999), it is not possible at the present stage to prefer the W to the homogeneous ISM case (H, hereafter). We already showed (Nava et al. 2006) that the collimation corrected $E_{\rm peak}$–E_γ correlation (so called 'Ghirlanda' correlation; Ghirlanda, Ghisellini & Lazzati 2004) has a smaller scatter and a linear slope when computed under the assumption of the W compared to the H case. It is, therefore, important to compare the estimates of Γ_0 and of the comoving frame energetics in these two possible scenarios. The most extensive study of Liang et al. (2010) estimated Γ_0 mostly from the peak of the afterglow light curve in the optical band and in few cases from a peak in the X-ray band. They considered only the H case and found a strong correlation between Γ_0 and the GRB isotropic equivalent energy $E_{\rm iso}$.

Equation (11) predicts that the afterglow light curve is flat in the coasting phase, with no peaks in the W density case ($s = 2$). However, this equation neglects pre-acceleration of the circumburst matter due to the prompt emission itself, which can have important consequences, as we discuss below.

4 HOMOGENEOUS OR WIND DENSITY PROFILE?

In the following we will find the initial bulk Lorentz factor Γ_0 for bursts showing a peak in their early afterglow light curve. In the simple case of an homogeneous circumburst density, we expect that the afterglow luminosity $L_{\rm aft} \propto t^2\Gamma^8$, and therefore $L_{\rm aft} \propto t^2$ when $\Gamma = \Gamma_0 =$ constant (equation 11). It can be questioned if, in the case of a wind density profile, such a peak occurs, or if the initial light curve is flat (i.e. $\propto t^0$), as suggested by equation (11) when $s = 2$.

The derivation leading to equation (11) assumes that the circumburst medium is at rest when the fireball impacts through it (i.e. it is an *external* shock). Instead, since the electrons in the vicinity of the burst scatter part of the prompt emission of the burst itself, some radial momentum has to be transferred to the medium (as suggested by Beloborodov 2002). If the velocity acquired by the circumburst matter becomes relativistic, then the fireball will produce an *internal* shock when passing through the medium, with a reduced efficiency.

To illustrate this point, let us consider an electron at some distance r from the burst, scattering photons of the prompt emission of energy $E_{\rm peak} = xm_{\rm e}c^2$. In the Thomson limit of the scattering process, this electron will scatter a number τ of prompt photons given by

$$\tau = \sigma_{\rm T} n_\gamma \Delta r = \frac{\sigma_{\rm T} L_{\rm iso} c t_{\rm burst}}{4\pi r^2 c\, x m_{\rm e} c^2} = \frac{\sigma_{\rm T} E_{\rm iso}}{4\pi r^2 x m_{\rm e} c^2}. \tag{16}$$

To evaluate the distance r up to which this process can be relevant, consider at what distance the electrons make a number $\tau \approx (m_{\rm p}/m_{\rm e})/x$ scatterings, namely the distance at which the electrons and their associated protons are accelerated to $\gamma \sim 2$:

$$r(\gamma = 2) \approx \left[\frac{\sigma_{\rm T} E_{\rm iso}}{4\pi m_{\rm p} c^2}\right]^{1/2} \sim 1.9 \times 10^{15} E_{\rm iso,53}^{1/2}\ {\rm cm} \tag{17}$$

where $E_{\rm iso,53} = 10^{53} E_{\rm iso}$ erg. This distance must be compared with the deceleration radius $r_{\rm dec}$ in the case of a wind density profile corresponding to a mass-loss $\dot{M}$ and a velocity $v_{\rm w}$ of the wind:

$$n(r) = \frac{\dot{M}}{4\pi r^2 m_{\rm p} v_{\rm w}} = 3.16 \times 10^{35} \frac{\dot{M}_{-5}}{v_{\rm w,8} r^2}, \quad (18)$$

where $\dot{M} = 10^{-5} \dot{M}_{-5}\, {\rm M}_\odot\, {\rm yr}^{-1}$ and $v_{\rm w} = 10^8\, {\rm cm\ s}^{-1}$ (i.e. $10^3\, {\rm km\, s}^{-1}$) (e.g. Chevalier & Li 1999). The deceleration radius is

$$r_{\rm dec} = \frac{E_{\rm iso}}{4\pi m_{\rm p} c^2 \eta \Gamma_0^2} \sim 1.7 \times 10^{16} \frac{E_{\rm iso,53} v_{\rm w,8}}{\eta_{-1} \dot{M}_{-5} \Gamma_{0,2}^2}\ {\rm cm}, \quad (19)$$

where η is the efficiency of conversion of the kinetic energy to radiation ($L_{\rm iso} = \eta L_{\rm k,iso}$). Therefore, it is possible to have a pre-acceleration of the circumburst matter up to a distance comparable to (but less than) the deceleration radius. In this case, we expect to have a very early *rising* afterglow light curve (corresponding to relatively inefficient internal shocks between the fireball and the pre-accelerated circumburst medium), followed by a flat light curve and then a decay.

We conclude that the absence of a flat early light curve does not exclude (a priori) a wind density profile. This gives us a motivation to explore both cases (i.e. homogeneous and wind density profile) even if the bursts in our sample all show a peak in the afterglow light curve (and thus a rising phase).

Note that the same pre-acceleration can occur if the density is homogeneous. In this case, again, we expect the very early afterglow to be less efficient than what predicted without pre-acceleration, leading to a rising phase even harder than t^2.

5 THE SAMPLE

Since we want to study the energetics, luminosities and peak energies of GRBs in the comoving frame, our first requirement is to know the redshift z. Then we also need that the spectral peak energy $E_{\rm peak}^{\rm obs}$ has been determined from the fit of the prompt emission spectrum. Most of these bursts have been localized by the Burst Alert Telescope (BAT; Barthelmy et al. 2005) on-board the *Swift* satellite, but only for a few of them BAT could determine $E_{\rm peak}^{\rm obs}$ (due to its limited energy range, 15–150 keV). Most of the $E_{\rm peak}^{\rm obs}$ were determined by the *Konus–Wind* satellite (Aptekar et al. 1995) or, since mid-2008, by the Gamma Burst Monitor (GBM; Meegan et al. 2009, with energy bandpass 8 keV–35 MeV) on-board the *Fermi* satellite. Our sample of GRBs with z and constrained $E_{\rm peak}^{\rm obs}$ (and consequently with computed $E_{\rm iso}$ and $L_{\rm iso}$) is updated up to 2011 May. It contains 132 GRBs with z, $E_{\rm peak}^{\rm obs}$ and $E_{\rm iso}$. We have $L_{\rm iso}$ for all but one of these bursts.

Within this sample, we searched the literature for bursts with evidence of the peak of the afterglow or an estimate of the Γ_0 factor.

(i) Liang et al. (2010, hereafter L10) measured the peaks in the optical light curves of GRBs and then estimated Γ_0 for the H case. From L10 we collected nine measurements of $t_{\rm p,z}$. L10 also collected other estimates of $t_{\rm p,z}$ from the literature (their table 6) from which we get other four values of this observable. Therefore, from L10 we collected 13 estimates of $t_{\rm p,z}$ from the optical light curves.

(ii) Two GRBs, not included in the sample of L10, that show a peak in their optical afterglow light curves are taken from Ghisellini et al. (2009).

(iii) L10 searched for bursts with evidence of the afterglow peak up to 2008 December. Our sample of bursts with redshifts, $E_{\rm peak}^{\rm obs}$ and isotropic energies/luminosities extends to 2011 May. We searched in the literature for $t_{\rm p,z}$ of bursts after 2008 December, and in 10 cases we could build the light curve with available published data (that will be presented in a forthcoming paper – Melandri et al., in preparation). Our systematic search of the literature resulted in other two GRBs with a peak in the optical light curve.

Our sample is thus composed of 27 GRBs with an estimate of $t_{\rm p,z}$ obtained from their optical light curves. All these are long GRBs.

The sample is presented in Table 1 where we show the relevant properties of these bursts used in the following sections. Columns 1 and 2 show the GRB name and its redshift, column 3 the rest frame peak energy $E_{\rm peak}$, and columns 4 and 5 the isotropic equivalent energy $E_{\rm iso}$ and luminosity $L_{\rm iso}$, respectively. In column 6 it is reported the rest frame $t_{\rm p,z}$ from which we compute the Γ_0 factor in the H case (column 7) and in the W case (column 8) assuming a typical density value $n_0 = 3\, {\rm cm}^{-3}$ or $n_0 = 3 \times 10^{35}\, {\rm cm}^{-1}$ (for the H and W, respectively) and a typical radiative efficiency $\eta = 0.2$. We note from equation (15) that the resulting Γ_0 is rather insensitive to the choice of n_0 and η both in the H case [i.e. $\Gamma_0 \propto (n_0\eta)^{-1/8}$] and in the W case [i.e. $\Gamma_0 \propto (n_0\eta)^{-1/4}$].

There are also four GRBs, detected by the Large Area Telescope (LAT) on-board *Fermi* at GeV energies, showing a peak in their GeV light curves (Ghisellini et al. 2010). The interpretation of the GeV emission as afterglow (Barniol-Duran & Kumar 2009, Ghirlanda et al. 2010b, Ghisellini et al. 2010) is however debated (Ackermann et al. 2010; Piran & Nakar 2010). Among these bursts there is also the short/hard GRB 090510 whose Γ_0 is derived from the modelling of the GeV light curve (Ghirlanda, Ghisellini & Nava 2010a). However, this burst also shows a clear peak in the optical at $\sim$300 s after the GRB onset (De Pasquale et al. 2010) which questions the afterglow interpretation of the GeV emission.

The three LAT bursts with $t_{\rm p,z}$ measured from the GeV light curve and the short GRB 090510 are shown separately in Table 1. These events have the smallest $t_{\rm p,z}$ in our sample and, therefore, the largest Γ_0 values (see Table 1). This is expected since, as discussed in Ghisellini et al. (2010), the detection in the GeV energy range by LAT seems to be a characteristic of GRBs with the largest values of $E_{\rm peak}^{\rm obs}$. Besides, the possible measure of $t_{\rm p,z}$ in the optical range is limited by the time delay of the follow-up of GRBs in this band, although several GRBs have been repointed in the optical band by Ultraviolet Optical Telescope on-board *Swift*. In the end, there could be a selection bias on the bursts with a peak in the GeV energy range, coupled with the debated interpretation of the GeV emission as afterglow. For these reasons, in the next sections we will present the results of the study of the correlations between the GRB energetics and Γ_0 both including and excluding these bursts. In all our quantitative analysis we always excluded the short GRB 090510 which is only shown for comparison with the properties of the 27 long GRBs.

In our sample we do not include upper limits on $t_{\rm p,z}$ which are those bursts observed early in the optical whose light curve is decaying up to several days without any sign of a peak. Several of these cases can be found in the literature and they would provide lower limits on the value of Γ_0. However, it is hard to define an appropriate sample of upper limits on $t_{\rm p,z}$ derived from the optical band because of the lack of a unique follow-up programme dedicated to the systematic observations of GRB afterglows.

6 RESULTS

In this section we first show the distributions of the Γ_0 factors computed in the H and W and show the correlation of Γ_0 with the

Table 1. The sample of GRBs with redshifts z, rest frame peak energy $E_{\rm peak}$, isotropic equivalent energy $E_{\rm iso}$ and luminosity $L_{\rm iso}$ (integrated in the 1 keV–10 MeV energy range) and peak time of the optical afterglow light curve (given in the source rest frame $t_{\rm p,z}$). The Γ_0 factors computed in the H and W cases are reported. The GRBs shown separately at the bottom of the table are the three long GRBs (080916C, 090902B and 090926A) showing a peak of the GeV light curve (as detected by *Fermi*-LAT), which could be interpreted as afterglow emission (Ghisellini et al. 2010). The short GRB 090510 is shown with two entries: one corresponding to the peak of the GeV light curve and the second to the peak of the optical light curve. The last column gives the references for the peak time of the afterglow: (1) Liang et al. (2010), peak of the optical light curve; (2) Liang et al. (2010), references in their table 6; (3) Ghisellini et al. (2010); (4) Ghisellini et al. (2009); (5) GRBs added in this work (Melandri et al., in preparation); (6) Gruber et al. (2011); (7) De Pasquale et al. (2010).

GRB	z	$E_{\rm peak}$ (keV)	$E_{\rm iso}$ (erg)	$L_{\rm iso}$ (erg s^{-1})	$t_{\rm p,z}$ (s)	$\Gamma_{\rm H}$	$\Gamma_{\rm W}$	Ref.
990123	1.60	2031 ± 161	(2.39 ± 0.28)E54	(3.53 ± 1.23)E53	18	312	182	2
030226	1.986	290 ± 63	(6.7±1.2)E52	(8.52 ± 2.23)E51	4340	26	19	5
050820A	2.612	1325 ± 277	(9.75 ± 0.77)E53	(91 ± 6.8)E51	108.17 ± 4.62	142	93	1
050922C	2.198	417 ± 118	(4.53 ± 0.78)E52	(190 ± 2.3)E51	42	138	55	2
060210	3.91	575 ± 186	(4.15 ± 0.57)E53	(59.5 ± 8.0)E51	97	133	77	2
060418	1.489	572 ± 114	(1.28 ± 0.10)E53	(18.9 ± 1.59)E51	60.73 ± 0.82	137	65	1
060605	3.78	490 ± 251	(2.83 ± 0.45)E52	(9.5 ± 1.5)E51	83.14 ± 2.7	101	41	1
060607A	3.082	575 ± 200	(10.9 ± 1.55)E52	(20 ± 2.7)E51	42.89 ± 0.62	153	68	1
060904B	0.703	135 ± 41	(36.4 ± 7.43)E50	(7.38 ± 1.4)E50	271.91 ± 33.75	50	18	1
061007	1.261	902 ± 43	(8.82 ± 0.98)E53	(17.4 ± 2.45E52	34.62 ± 0.18	215	121	1
061121	1.314	1289 ± 153	(2.61 ± 0.3)E53	(141 ± 1.5)E51	250	88	54	4
070110	2.352	370 ± 170	(5.5 ± 1.5)E52	(45.1 ± 7.52)E50	350	64	34	4
071010B	0.947	101 ± 23	(2.12 ± 0.36)E52	(64 ± 0.53)E50	67	105	40	2
080319C	1.95	1752 ± 505	(15 ± 0.79)E52	(9.5 ± 0.12)E52	117.38 ± 3.22	109	57	1
080804	2.2	810 ± 45	(1.15 ± 0.2)E53	(2.69 ± 0.32)E52	40.5	157	70	5
080810	3.35	1488 ± 348	(3.91 ± 0.37)E53	(9.27 ± 0.87)E52	27.02 ± 0.26	214	105	1
081203A	2.1	1541 ± 757	(3.5 ± 0.3)E53	(28.1 ± 1.94)E51	118.09 ± 0.46	121	70	1
090102	1.547	1148 ± 143	(2.2 ± 0.26)E53	(8.7 ± 0.56)E52	20.3	221	97	5
090618	0.54	155.5 ± 11	(2.53 ± 0.25)E53	(2.05 ± 0.1)E52	51.9	158	80	5
090812	2.452	2023 ± 663	(4.03 ± 0.4)E53	(95.6 ± 9.66)E51	17.38	253	118	5
091024	1.092	794 ± 231	(2.8 ± 0.3)E53	(1.0 ± 0.22)E52	1912	59	66	6
091029	2.752	230 ± 66	(7.4 ± 0.74)E52	(13.2 ± 0.73)E51	88	111	51	5
100621A	0.542	146 ± 23.1	(4.37 ± 0.5)E52	(3.16 ± 0.24)E51	3443	26	18	5
100728B	2.106	404 ± 29	(3.0 ± 0.3)E52	(18.6 ± 1.20)E51	16	188	63	5
100906A	1.727	158 ± 16	(3.34 ± 0.3)E53	(24.5 ± 0.86)E51	37	186	93	5
110205A	2.22	715 ± 239	(5.6 ± 0.6)E53	(2.50 ± 0.34)E52	311	89	62	5
110213A	1.46	241 ± 13	(6.4 ± 0.6)E52	(20.9 ± 0.58)E51	81	113	51	5
080916C	4.35	2759 ± 120	(5.6 ± 0.5)E54	(10.4 ± 0.88)E53	1.5	880	419	3
090510	0.903	4400 ± 400	(5.0 ± 0.5)E52	(1.78 ± 0.12)E53	0.44(315.3)	773(66)	175(34)	3(7)
090902B	1.822	2020 ± 17	(44 ± 0.3)E53	(58.9 ± 0.97)E52	3.2	643	327	3
090926A	2.106	907 ± 7	(20 ± 0.52)E53	(74 ± 1.45)E52	2.9	605	275	3

isotropic energy $E_{\rm iso}$ and luminosity $L_{\rm iso}$. Then we show how the distributions of $E_{\rm peak}$, $E_{\rm iso}$ and $L_{\rm iso}$ change when they are corrected for the Γ_0 factor, i.e. how they appear in the comoving frame ($E'_{\rm peak}$, $E'_{\rm iso}$, $L'_{\rm iso}$). In doing this, we always consider the two estimates of Γ_0 in the H and W to compare the different distributions of the spectral parameters. Finally, we present the rest frame $E_{\rm peak}$–$E_{\rm iso}$ and $E_{\rm peak}$–$L_{\rm iso}$ correlations (updated here with 132 and 131 GRBs up to 2011 May) and, for those bursts in our sample with measured Γ_0, we show where they cluster in these planes when the beaming corrections [$E'_{\rm peak} = E_{\rm peak}/(5\Gamma/3)$, $E'_{\rm iso} = E_{\rm iso}/\Gamma$, $L'_{\rm iso} = L_{\rm iso}/(4\Gamma^2/3)$] are applied.

For all the reasons outlined in Section 5, in the following we consider (i) the optical sample of 27 GRBs with measured z, $E^{\rm obs}_{\rm peak}$, $E_{\rm iso}$ and $L_{\rm iso}$, whose $t_{\rm p,z}$ is measured from the optical light curve and (ii) the extended sample of 30 GRBs which includes the three long GRBs with a peak in the GeV which, if interpreted as afterglow emission, allows us to estimate the largest Γ_0 in our sample.

6.1 Γ_0 distributions

Fig. 1 shows the distributions of the Γ_0 factors of the 27 GRBs of our sample (with $t_{\rm p,z}$ measured from the optical light curve – Table 1) computed in the H (solid histogram) and W (hatched histogram) cases, respectively. The two distributions are fitted with Gaussian functions and the central value and dispersion are reported in Table 2. The average Γ_0 factor is ∼138 in the H case and ∼66 in the W case. In both the H and W cases, the distribution of Γ_0 is broad, spanning nearly one decade.

6.2 $E_{\rm iso}$–Γ_0, $L_{\rm iso}$–Γ_0, $E_{\rm peak}$–Γ_0 correlations

In this section we explore the presence of correlations between the rest frame GRB properties (i.e. the peak energy $E_{\rm peak}$, the isotropic equivalent energy $E_{\rm iso}$ and luminosity $L_{\rm iso}$) and the Γ_0 factor.

In the upper panels of Fig. 2 we show the isotropic energy $E_{\rm iso}$ and luminosity $L_{\rm iso}$ (open red circles and filled green squares, respectively) as a function of Γ_0 in both the H and W cases (left- and right-hand panels, respectively). In the bottom panels of Fig. 2 we show the peak energy $E_{\rm peak}$ as a function of Γ_0 in the H (left-hand panel) and W (right-hand panel) cases.

The Spearman rank correlation coefficients and associated chance probabilities are reported in Table 3. We model the correlations with a power law: $\log Y = m \log \Gamma_0 + q$ (with $Y = E_{\rm iso}$, $Y = L_{\rm iso}$ or $Y = E_{\rm peak}$) and list the best-fitting parameters in Table 3. We fit this

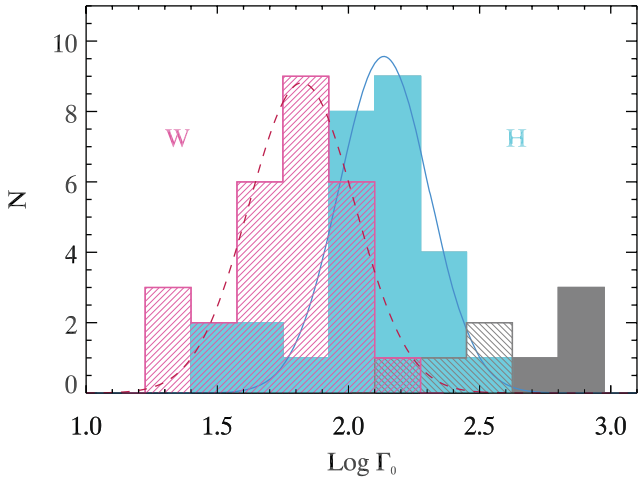

Figure 1. Γ_0 distributions of the 31 GRBs in the case of an homogeneous ISM (H – solid filled blue histogram) and in the case of a wind density profile (W – hatched histogram). The Gaussian functions show the fits (solid and dashed line for the H and W cases, respectively) to the histograms of the sample of 27 GRBs with $t_{p,z}$ derived from the optical light curve. The three long and one short GRBs with $t_{p,z}$ measured from the GeV light curve are shown by the grey solid and hatched histograms, for the H and W cases respectively, but are not included in the fits.

Table 2. Central values and dispersions of the Gaussians fitted to the distributions of Γ_0, E_{peak} and E'_{peak}, E_{iso} and E'_{iso}, L_{iso} and L'_{iso}. For each quantity we report the Gaussian fits to the sample of 27 GRBs with $t_{p,z}$ measured from the optical light curve and the sample of 30 GRBs which includes the three events with $t_{p,z}$ measured from the GeV light curve, if interpreted as afterglow. The short GRB 090510 has been excluded from this analysis.

	Parameter	#GRBs	Central value	Dispersion (σ)
	$\log E_{peak}$	132	2.68	0.43
		27	2.81	0.50
		30	2.85	0.35
	$\log E_{iso}$	132	53.05	0.77
		27	53.19	0.64
		30	53.25	0.71
	$\log L_{iso}$	131	52.46	0.73
		27	52.53	0.82
		30	52.62	0.87
Density				
H	$\log \Gamma_0$	27	2.14	0.17
		30	2.14	0.18
	$\log E'_{peak}$	27	0.49	0.35
		30	0.44	0.38
	$\log E'_{iso}$	27	51.14	0.49
		30	51.22	0.55
	$\log L'_{iso}$	27	48.12	0.47
		30	48.11	0.39
W	$\log \Gamma_0$	27	1.82	0.20
		30	1.82	0.21
	$\log E'_{peak}$	27	0.79	0.24
		30	0.76	0.27
	$\log E'_{iso}$	27	51.47	0.43
		30	51.54	0.45
	$\log L'_{iso}$	27	48.69	0.26
		30	48.71	0.23

model to the data points (shown in Fig. 2) with the bisector method. The choice of this fitting method, instead of the least square Y versus X method that minimizes the vertical distances of the data from the fitting line, is motivated by the large dispersion of the data and the absence of any physical motivation for assuming that Γ_0 or instead E_{iso}, L_{iso} or E_{peak} are the independent variable (Isobe et al. 1990).

In a recent work, Lv, Zou & Lei (2011) derive a correlation $\Gamma_0 \propto E_{iso}^{0.22}$, similar to that found in L10. Such a flat correlation is obtained because Γ_0 is fitted versus E_{iso} (or L_{iso}). As described above, the large scatter of the correlations and the lack of any physical reason for assuming either Γ_0 or E_{iso} (L_{iso}) as the independent variable require instead that these correlations are fitted with the bisector method. This gives different correlation slopes with respect to those reported in L10 and Lv et al. (2011). Moreover, in our sample we only consider bursts with firm estimates of E_{peak} and do not include those GRBs which are fitted by a simple power law in the BAT energy range but whose peak energy is derived through a Bayesian method, based on the properties of bright BATSE bursts (Butler et al. 2007).

We find that there are strong correlations between the spectral peak energy and isotropic energy/luminosity with Γ_0. The slopes of these correlations are rather insensitive to the circumburst profile adopted in deriving Γ_0 (H or W) and are similar for E_{iso} and L_{iso} ($E_{iso} \propto \Gamma_0^2$ and $L_{iso} \propto \Gamma_0^2$). A roughly linear correlation exists between E_{peak} and Γ_0: $E_{peak} \propto \Gamma_0$ (bottom panels in Fig. 2).

The dispersion of the data points around the best-fitting correlations (shown by the solid and dashed lines in Fig. 2) is modelled with a Gaussian and its σ_{sc} is given in Table 3. The less dispersed correlation is between the luminosity L_{iso} and Γ_0 (with $\sigma_{sc} = 0.07$).

We finally verified that there is no correlation between the GRB duration T_{90} and Γ_0 (chance probability $P = 0.3$ and 0.7 for the H and W cases) and between the redshift z and Γ_0.

6.3 Comoving frame E'_{peak}, E'_{iso}, L'_{iso} distributions

In Figs 3, 4 and 5 we show the distributions of the comoving frame peak energy, isotropic equivalent energy and luminosity. In Fig. 3 we show the distributions of the peak energy: the sample of 132 GRBs with measured redshifts and known E_{peak} is shown with the dashed line and the subsample of 30 GRBs of this work for which we could estimate Γ_0 is shown with the red hatched histograms. These distributions represent E_{peak}, i.e. the peak energy in the rest frame of the sources.

The distributions of the comoving peak energy [derived as $E'_{peak} = E_{peak}/(5\Gamma_0/3)$] are shown by the (cyan) filled and hatched (purple) histograms in Fig. 3 for the H and W cases, respectively, considering the 27 GRBs which show a peak in the optical light curve. Fig. 3 shows also the fits with Gaussian functions: their parameters are reported in Table 2.

There is a reduction of the dispersion of the distribution of the peak energy from the rest frame to the comoving one. In the comoving frame E'_{peak} clusters around ∼6 and ∼3 keV in the H and W cases, respectively, with dispersions of nearly one decade, i.e. narrower than the dispersion of E_{peak}.

Fig. 4 shows the distribution of the isotropic energy E_{iso} for all the 132 GRBs with known z and measured E_{peak} (dashed line) and for the 30 GRBs with an estimate of Γ_0 (hatched red histogram). The $E'_{iso} = E_{iso}/\Gamma_0$ distributions are shown with the solid filled (cyan) histogram and the hatched (purple) histogram for the H and W cases. These distributions are obtained with the 27 GRBs with a

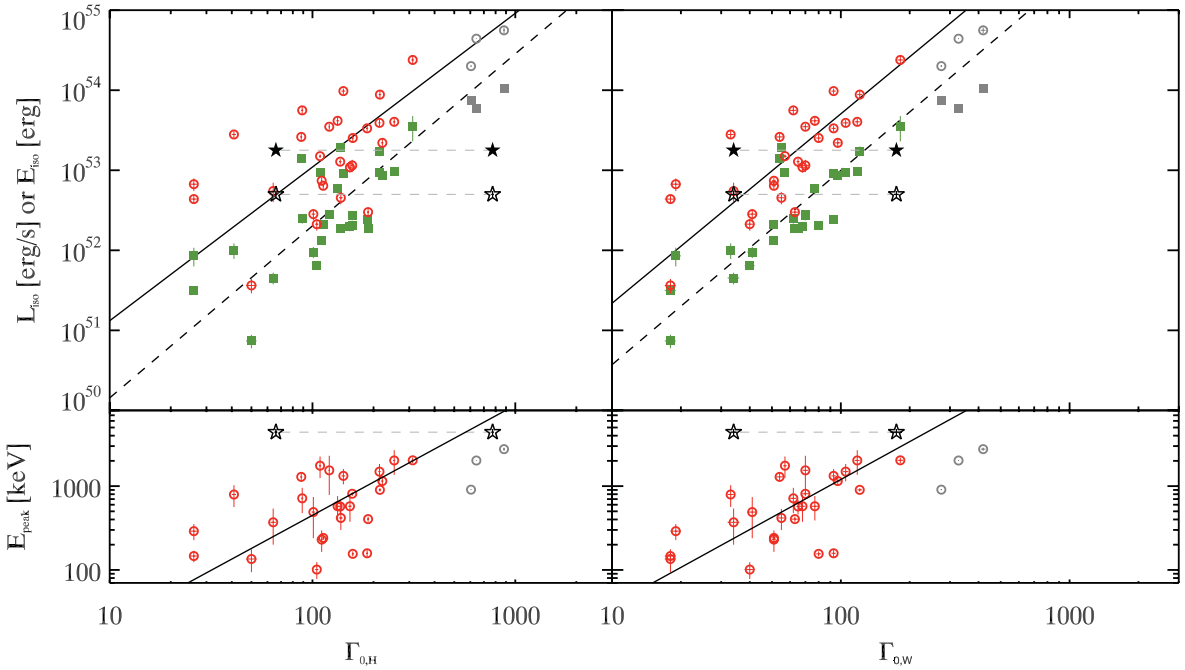

Figure 2. Top panels: isotropic equivalent energy E_{iso} (open circles) and luminosity L_{iso} (filled squares) as a function of Γ_0, computed for the 30 GRBs in our sample in the H case (left-hand panel) and W case (right-hand panel). The solid (dashed) line in both panels show the least-squares fit with a power law to the E_{iso}–Γ_0 (L_{iso}–Γ_0) correlation to the sample of 27 GRBs with peak in the optical light curve (open red circles and filled green squares). The three GRBs with peak in the GeV light curve are shown with the grey symbols, but are not included in the fits shown here. The short GRB 090510 with both a peak in the GeV and a delayed peak in the optical (see Table 1) is shown by star symbols connected by the dashed (grey) line. The larger value of Γ_0 is that derived from the peak in the GeV light curve. Bottom panels: peak energy E_{peak} for the H case (left-hand panel) and W case (right-hand panel) as a function of Γ_0. The solid line is the best-fitting correlation. The correlation coefficient and the slope and normalization of the best-fitting correlations are reported in Table 3.

Table 3. Results of the fit of the Γ_0–E_{iso}, Γ_0–L_{iso} and Γ_0–E_{peak} correlations in the two cases of homogeneous ISM (H) and wind density profile (W). The Spearman correlation coefficient ρ and the chance probability P_{chance} are reported together with the slope m and normalization q of the fit of the data points with a linear model. The fit is done with the bisector method considering the sample of 27 GRBs with optical peak and the 30 GRBs (i.e. including the three long bursts with peak in the GeV).

Correlation	#GRBs	ρ	P_{chance}	m	q	σ_{sc}
E_{iso}–Γ_0^H	27	0.48	10^{-2}	1.92 ± 0.40	49.20 ± 0.88	0.28
	30	0.74	2.5×10^{-4}	1.96 ± 0.26	49.11 ± 0.62	0.23
L_{iso}–Γ_0^H	27	0.64	3×10^{-4}	2.15 ± 0.34	48.01 ± 0.74	0.18
	30	0.74	3×10^{-6}	2.04 ± 0.22	48.21 ± 0.51	0.20
E_{peak}–Γ_0^H	27	0.45	10^{-2}	1.31 ± 0.2	0.03 ± 0.36	0.21
	30	0.56	10^{-3}	1.13 ± 0.13	0.36 ± 0.31	0.23
E_{iso}–Γ_0^W	27	0.75	4×10^{-4}	2.36 ± 0.36	48.97 ± 0.60	0.18
	30	0.82	2.2×10^{-8}	2.15 ± 0.20	49.32 ± 0.42	0.10
L_{iso}–Γ_0^W	27	0.76	5×10^{-6}	2.40 ± 0.24	48.14 ± 0.43	0.07
	30	0.82	2.6×10^{-8}	2.19 ± 0.16	48.52 ± 0.31	0.10
E_{peak}–Γ_0^W	27	0.62	5×10^{-4}	1.50 ± 0.20	0.08 ± 0.30	0.25
	30	0.69	2.3×10^{-5}	1.21 ± 0.20	0.54 ± 0.27	0.31

peak in the optical light curve. The three GRBs with a peak in the GeV light curve are only shown for comparison (hatched and filled grey histograms). The distributions of E'_{iso} are wide. On average, the comoving frame $E'_{iso} \sim 1$–3×10^{51} erg in both the H and W cases, but there is a reduction of the dispersion of the distribution of E_{iso} from the rest ($\sigma_{sc} = 0.64$) to the comoving frame ($\sigma_{sc} = 0.43$ and 0.49) for the W and H cases, respectively (see Table 2).

Finally, in Fig. 5 we show the distribution of L_{iso} for the 131 GRBs in the sample (dashed line), the distribution of L_{iso} for the 30 GRBs with estimated Γ_0 (red hatched histogram) and the comoving frame $L'_{iso} = L_{iso}/(4\Gamma_0^2/3)$ distribution (solid filled cyan and hatched purple histograms for the H and W cases, respectively, obtained with the 27 GRBs with a peak in the optical light curve). Interestingly, we find a strong clustering of the comoving frame distribution of L'_{iso}. For the H case we find (see Table 2 for the values of the Gaussian fits) an average $L'_{iso} \sim 10^{48}$ erg s^{-1} with a small dispersion (0.47 dex), while when using the Γ_0 computed in the wind density profile (W) case we find an almost universal value of $L'_{iso} \sim 5 \times 10^{48}$ erg s^{-1} with a dispersion of less than 1 order of magnitude around this value (hatched purple histogram and dashed purple line in Fig. 5).

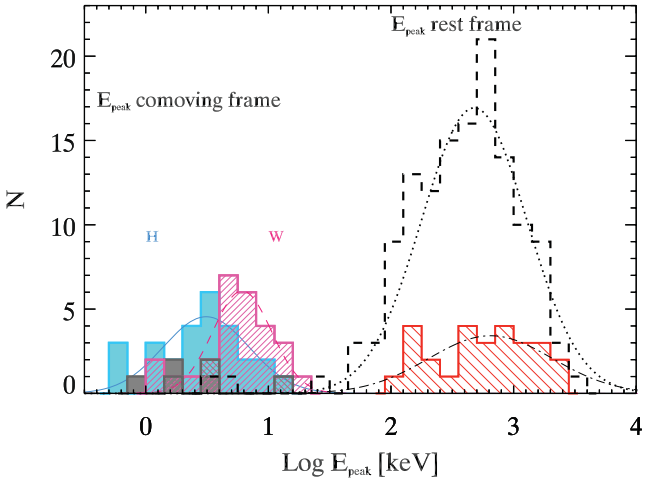

Figure 3. Peak energy distributions in the rest frame $E_{\rm peak}$ (dashed histogram) for the sample of 132 GRBs with known redshift and constrained $E_{\rm peak}$. The hatched histogram shows the 30 GRBs of our sample for which we have an estimate of the peak of the afterglow and hence of Γ_0. The beaming-corrected distribution of $E'_{\rm peak} = E_{\rm peak}/(5\Gamma_0/3)$ is shown by the solid filled (cyan) histogram in the H case and with the hatched (purple) histogram in the W case. For all the distributions, we also show the Gaussian fits whose parameters are reported in Table 2. The four GRBs with a peak in the GeV light curve are shown with grey filled and hatched histograms.

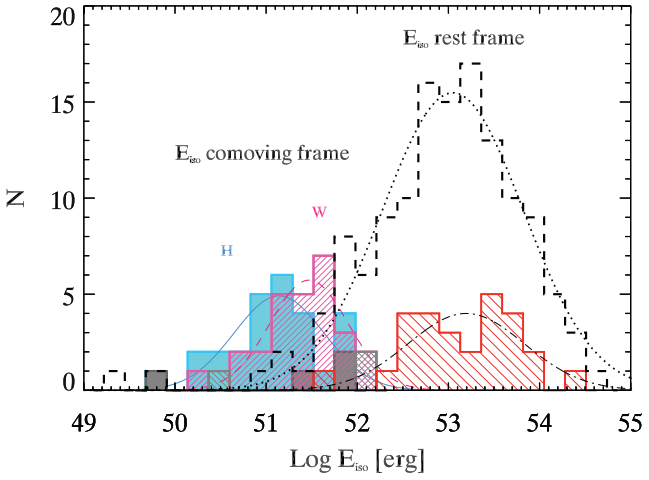

Figure 4. Isotropic energy distributions in the rest frame (dashed histogram) for the sample of 132 GRBs with known redshift and constrained $E^{\rm obs}_{\rm peak}$. The hatched histogram shows the 30 GRBs of our sample for which we have an estimate of the peak of the afterglow. The beaming-corrected distribution of $E'_{\rm iso} = E_{\rm iso}/\Gamma_0$ is shown by the solid filled histogram and hatched purple histogram for the H and W cases for the 27 GRBs with a peak in the optical light curve. The four GRBs with a peak in the GeV light curve are shown for comparison with the hatched and filled grey histograms.

6.4 Comoving frame $E'_{\rm peak}$–$E'_{\rm iso}$ and $E'_{\rm peak}$–$L'_{\rm iso}$ correlations

Here we show the effect of correcting the spectral energy correlations $E_{\rm peak}$–$E_{\rm iso}$ and $E_{\rm peak}$–$L_{\rm iso}$ for the bulk Lorentz factors Γ_0. These correlations were originally found with a dozen of GRBs [Amati et al. (2002) and Yonetoku et al. (2004) for the $E_{\rm peak}$–$E_{\rm iso}$ and $E_{\rm peak}$–$L_{\rm iso}$ correlations, respectively] and since then updated with newly discovered GRBs with measured redshifts z and well-constrained spectral peak energies $E_{\rm peak}$. In this work we have updated the sample of GRBs with all these observables up to 2011 May. We have 132 GRBs with measured z and known $E_{\rm peak}$ and $E_{\rm iso}$ and 131 GRBs with measured z and $E_{\rm peak}$ and $L_{\rm iso}$. We show the corresponding $E_{\rm peak}$–$E_{\rm iso}$ and $E_{\rm peak}$–$L_{\rm iso}$ correlations in Fig. 6 (left- and right-hand panels, respectively). The best-fitting correlation parameters (obtained with the bisector method) are reported in Table 4. We find that $E_{\rm peak} \propto E_{\rm iso}^{0.56}$ (dashed line in Fig. 6) with a scatter $\sigma = 0.24$ (computed perpendicular to the best-fitting line and modelled with a Gaussian function). The other correlation is $E_{\rm peak} \propto L_{\rm iso}^{0.50}$ with a slightly larger scatter $\sigma = 0.3$. The 1σ, 2σ and 3σ dispersion of the correlations are shown with the shaded stripes.

Fig. 6 also shows the comoving frame $E'_{\rm peak}$ and $E'_{\rm iso}$ (left-hand panel) and $E'_{\rm peak}$ and $L'_{\rm iso}$ (right-hand panel) for the 30 GRBs of our sample with an estimate of Γ_0 in the H case. The 27 GRBs with a peak in the optical are shown with the cyan filled squares in Fig. 6, while the three long GRBs with a peak in the GeV light curve are shown with the filled grey squares. Fig. 7 shows the same correlations ($E_{\rm peak}$–$E_{\rm iso}$ and $E_{\rm peak}$–$L_{\rm iso}$ in the left- and right-hand panels, respectively) for the W case. We note that in both the H and W cases there is a clustering of the points around typical values of $E'_{\rm peak}$, $E'_{\rm iso}$ and $L'_{\rm iso}$. Table 4 reports the correlation analysis among the comoving frame quantities.

7 DISCUSSION AND CONCLUSIONS

We have considered all bursts with measured $E_{\rm peak}$ and known redshift up to May 2011 (132 GRBs). Among these we have searched in the literature for any indication of the peak of the afterglow light curve $t_{\rm p,z}$ suitable to estimate the initial bulk Lorentz factor Γ_0. Our sample of bursts is composed by 27 GRBs with a clear evidence of $t_{\rm p,z}$ in the optical light curve. We have derived the peak energy $E'_{\rm peak}$, the isotropic energy $E'_{\rm iso}$ and the isotropic peak luminosity $L'_{\rm iso}$ in the comoving frame. To this aim we have derived the general formula for the computation of Γ_0 (Section 3) considering two possible scenarios: a uniform ISM density profile ($n = {\rm const}$, H) or a wind density profile ($n \propto r^{-2}$, W).

For the wind case, the Γ_0 distribution (Fig. 1 and Table 2) is shifted at somewhat smaller values ($\langle\Gamma_0\rangle \sim 66$) than the same distribution for the homogeneous density case ($\langle\Gamma_0\rangle \sim 138$). The distribution of $E'_{\rm peak}$ is relatively narrow and centred around $\sim$6 or $\sim$3 keV for the W and H cases (Fig. 3 and Table 2). The distribution of $L'_{\rm iso}$ (Fig. 5) clusters, especially for the wind case, in a very narrow range (much less than a decade), around 5×10^{48} erg s^{-1}, while the distribution of $E'_{\rm iso}$ (Fig. 4) is broader and centred at 3×10^{51} erg. $E_{\rm iso}$ and $L_{\rm iso}$ correlate with Γ_0 ($\propto \Gamma_0^{2.2}$ both for the wind and the homogeneous case) and the correlation is stronger (with a scatter $\sigma = 0.07$) for the wind case. Finally, the duration of the burst, as expected, does not correlate with Γ_0.

The correlations that we have found are strong despite they are defined with a still small number of GRBs. We expect that with the increase of the number of GRBs with measured $t_{\rm p,z}$ and well-determined spectral properties (i.e. $E_{\rm peak}$, $E_{\rm iso}$ and $L_{\rm iso}$) the slope and normalization of these correlations might change.

For comparison we also considered four GRBs with a peak in the GeV light curve. If the GeV emission is interpreted as afterglow (Barniol-Duran & Kumar 2009; Ghirlanda et al. 2010b; Ghisellini et al. 2010), the measure of $t_{\rm p,z}$ at early times in the GeV range allows us to estimate their Γ_0 that are consistent with the correlations found using only the bursts with $t_{\rm p,z}$ observed in the optical. Although not a proof, this is a hint in favour of the afterglow origin of the GeV emission.

These results are schematically summarized in the first column of Table 5. The second column of the same table reports some

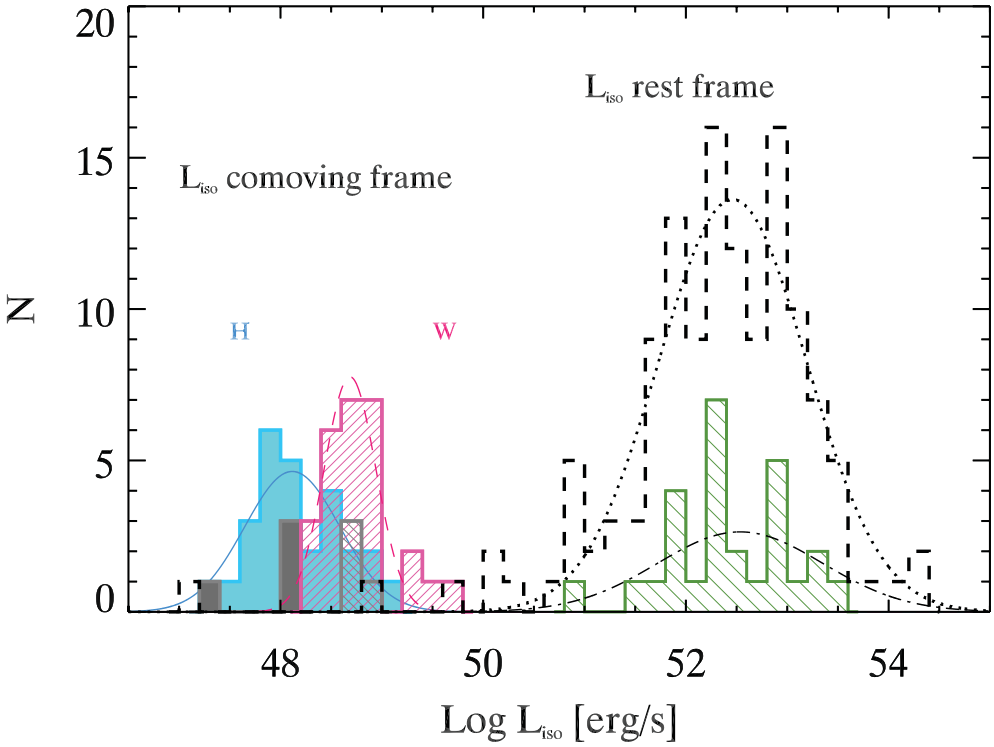

Figure 5. Isotropic luminosity distributions in the rest frame (dashed histogram) for the sample of 131 GRBs with known redshift and constrained $E_{\rm peak}^{\rm obs}$. The hatched histogram shows the 30 GRBs of our sample for which we have an estimate of the peak of the afterglow. The beaming-corrected distribution of $L'_{\rm iso}$ is shown by the solid filled histogram and hatched purple histogram for the H and W cases for the 27 GRBs with a peak in the optical light curve. The four bursts with a peak in the GeV light curve are shown for comparison with the hatched and filled grey histograms.

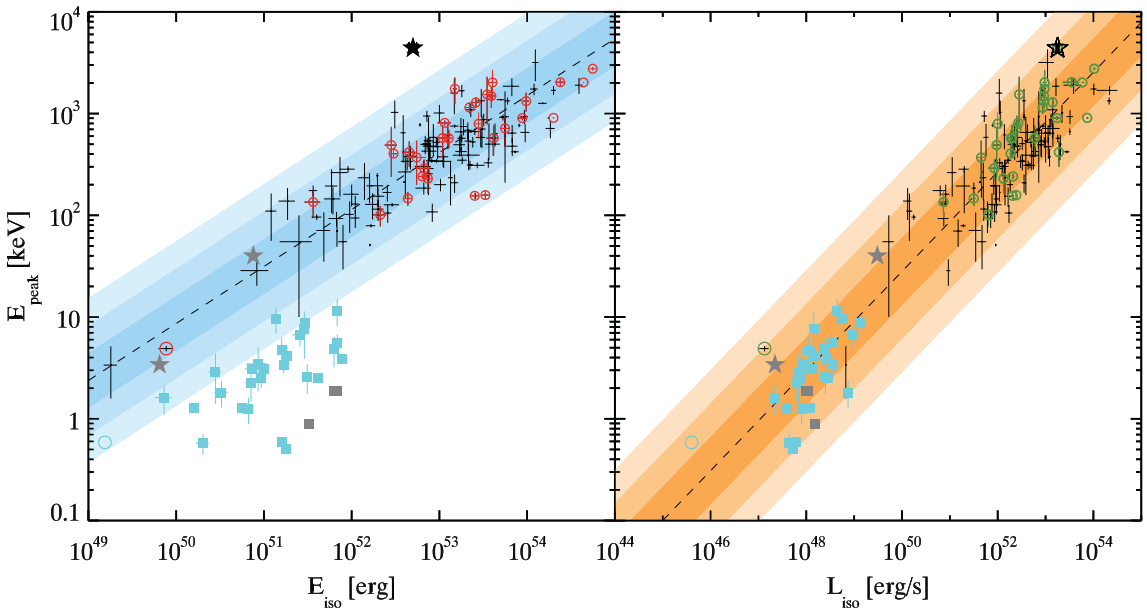

Figure 6. Homogeneous ISM (H). Left: $E_{\rm peak}$–$E_{\rm iso}$ correlation in the rest frame (crosses and red circles) for 132 GRBs with z and fitted $E_{\rm peak}$ updated up to 2011 May. Right: $E_{\rm peak}$–$L_{\rm iso}$ correlation with 131 GRBs. In both panels, the best-fitting correlation is shown by the dashed line and its 1σ, 2σ, 3σ scatters are shown by the shaded region. The comoving frame $E'_{\rm peak}$ and $E'_{\rm iso}$ (left) and $E'_{\rm peak}$ and $L'_{\rm iso}$ (right) of 30 GRBs [red open circles (left-hand panel) and green open circles (right-hand panel)] in our sample (Table 1) with an estimate of the Γ_0 factor are shown with the filled cyan square symbols (27 events with $t_{\rm p,z}$ in the optical light curve) or grey filled square (the three long GRBs with a peak in the GeV light curve). The short GRB 090510 is also shown with a star symbol and the low-luminosity GRB 060218 (with $\Gamma_0 \sim 5$; Ghisellini, Ghirlanda & Tavecchio 2007) is shown with an open circle.

Table 4. Results of the fit of the $E_{\rm peak}$–$E_{\rm iso}$ and $E_{\rm peak}$–$L_{\rm iso}$ correlations updated in this paper up to May 2011. The Spearman correlation coefficient ρ and the chance probability $P_{\rm chance}$ are given with the slope m and normalization q of the least-squares fit.

	Correlation	#GRBs	ρ	$P_{\rm chance}$	m	q	$\sigma_{\rm sc}$
	$E_{\rm peak}$–$E_{\rm iso}$	132	0.8	10^{-30}	0.56 ± 0.02	-26.06 ± 1.14	0.24
	$E_{\rm peak}$–$E_{\rm iso}$	27	0.71	3×10^{-5}	0.67 ± 0.10	-33.88 ± 5.0	0.28
	$E_{\rm peak}$–$E_{\rm iso}$	30	0.76	10^{-6}	0.58 ± 0.07	-28.26 ± 3.74	0.29
	$E_{\rm peak}$–$L_{\rm iso}$	131	0.77	3×10^{-26}	0.49 ± 0.04	-23.03 ± 1.84	0.30
	$E_{\rm peak}$–$L_{\rm iso}$	27	0.76	3×10^{-6}	0.65 ± 0.08	-31.53 ± 4.36	0.25
	$E_{\rm peak}$–$L_{\rm iso}$	30	0.8	10^{-7}	0.57 ± 0.06	-27.14 ± 3.37	0.27
Density	Correlation	#GRBs	ρ	$P_{\rm chance}$			
H	$E'_{\rm peak}$–$E'_{\rm iso}$	27	0.62	6×10^{-4}			
	$E'_{\rm peak}$–$E'_{\rm iso}$	30	0.43	2×10^{-2}			
	$E'_{\rm peak}$–$L'_{\rm iso}$	27	0.72	2×10^{-5}			
	$E'_{\rm peak}$–$L'_{\rm iso}$	30	0.68	3×10^{-5}			
W	$E'_{\rm peak}$–$E'_{\rm iso}$	27	0.41	4×10^{-2}			
	$E'_{\rm peak}$–$E'_{\rm iso}$	30	0.28	0.3			
	$E'_{\rm peak}$–$L'_{\rm iso}$	27	0.50	7×10^{-3}			
	$E'_{\rm peak}$–$L'_{\rm iso}$	30	0.47	10^{-2}			

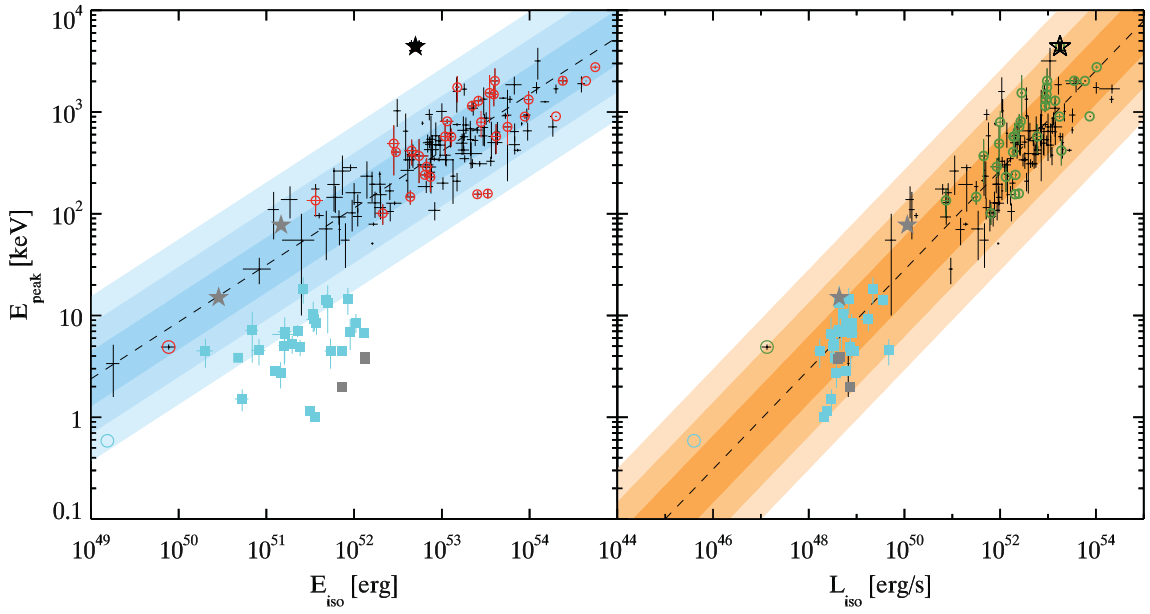

Figure 7. Wind ISM (W). Same as Fig. 6.

Table 5. Schematic summary of our results and their implications for the case of a wind density profile. We have assumed that both $E_{\rm iso}$ and $L_{\rm iso}$ scale as Γ^2, instead of $\Gamma^{2.2}$.

Our results	Implications	If $\theta_{\rm j}^2\Gamma \sim$ const
$E'_{\rm peak} \sim$ const	$E_{\rm peak} \propto \Gamma$	
$E_{\rm iso} \propto \Gamma^2$	$E_{\rm iso} \propto E_{\rm peak}^2$	$E_\gamma = \theta_{\rm j}^2 E_{\rm iso} \propto \Gamma \propto E_{\rm peak}$
$L_{\rm iso} \propto \Gamma^2$	$L_{\rm iso} \propto E_{\rm peak}^2$	$L_\gamma = \theta_{\rm j}^2 L_{\rm iso} \propto \Gamma \propto E_{\rm peak}$
T_{90} not $f(\Gamma)$	$T'_{90} \propto \Gamma$	$E'_\gamma \sim$ const
$L'_{\rm iso} \sim$ const	$E'_{\rm iso}/L'_{\rm iso} \propto T'_{90} \propto \Gamma$	$L'_\gamma \sim E'_\gamma/T'_{90} \sim 1/\Gamma$

immediate implications of these results. Since $E'_{\rm peak} \propto E_{\rm peak}\Gamma_0$ is contained in a narrow range, all bursts emit their radiation at a characteristic frequency in their comoving frame, irrespective of their bulk Lorentz factor. Furthermore, we can assume that $E_{\rm peak} \propto \Gamma_0$, and this, together with the quadratic dependence on Γ_0 of $E_{\rm iso}$ and $L_{\rm iso}$, yields the 'Amati' and the 'Yonetoku' relations. *They are the result of a different* Γ_0 *factors.* Indeed, at the extremes of the $E_{\rm peak}$–$E_{\rm iso}$ and $E_{\rm peak}$–$L_{\rm iso}$ correlations we find GRB 060218 which has the lowest $\Gamma_0 \sim 5$ (inferred from its X-ray and optical properties – Ghisellini et al. 2007), while at the upper end (corresponding to the largest peak energies and isotropic energetics and luminosities) there is GRB 080916C which has the largest

$\Gamma_0 = 880$. The fact that the $E_{\rm peak}$–$E_{\rm iso}$ and $E_{\rm peak}$–$L_{\rm iso}$ correlations could be a sequence of Γ_0 factors has been also proposed by Dado, Dar & De Rujula (2007) based on different assumptions.

If all bursts had the same jet opening angle, then $L'_\gamma = \theta_{\rm j}^2 L'_{\rm iso}$, and the (logarithmic) width of the $L'_{\rm iso}$ distribution would be the same of the (more fundamental) L'_γ distribution. On the other hand, we have some hints that very energetic and luminous GRBs tend to have narrower opening angles (e.g. Firmani et al. 2005). It is this property that makes the collimation corrected E_γ and L_γ quantities to correlate with $E_{\rm peak}$ in a different way (i.e. different slope) than in the Amati and Yonetoku relations (Ghirlanda et al. 2004; Nava et al. 2006).

We are then led to propose the following ansatz: the opening angle of the jet inversely correlates with the bulk Lorentz factor $\theta_{\rm j} \propto \Gamma_0^{-a}$. There are too few GRBs in our sample with measured $\theta_{\rm j}$ to find a reasonable value for the exponent a, but it is nevertheless instructive to explore the case $a = 1/2$, leading to $\theta_{\rm j}^2\Gamma_0 =$ constant. If we assume this relation, we find, for the collimation corrected E_γ,

$$E_\gamma = \theta_{\rm j}^2 E_{\rm iso} \propto \Gamma_0 \propto E_{\rm peak}. \quad (20)$$

This is the 'Ghirlanda' relation in the wind case (Nava et al. 2006). Similarly, for the collimation corrected luminosity (Ghirlanda, Ghisellini & Firmani 2006):

$$L_\gamma = \theta_{\rm j}^2 L_{\rm iso} \propto \Gamma_0 \propto E_{\rm peak}. \quad (21)$$

Another important consequence of our ansatz is that, in the comoving frame, the collimation corrected energetic E'_γ becomes constant:

$$E'_\gamma = \theta_{\rm j}^2 \frac{E_{\rm iso}}{\Gamma_0} = \text{ constant}. \quad (22)$$

This allows us to 're-interpret' the constancy of $L'_{\rm iso}$ as a consequence of the constant E'_γ:

$$L'_{\rm iso} \sim \frac{E'_\gamma}{T'_{90}\theta_{\rm j}^2} = \frac{E'_\gamma}{T_{90}\theta_{\rm j}^2\Gamma_0} = \text{ constant}. \quad (23)$$

In other words, in the comoving frame, the burst emits *the same amount of energy at the same peak frequency*, irrespective of the bulk Lorentz factor. For larger Γ_0 the emitting time in the comoving frame is longer (by a factor Γ_0 if the observed T_{90} is the same), so the comoving luminosity is smaller. But since the jet opening angle is also smaller (for larger Γ_0), the isotropic equivalent luminosity turns out to be the same. These consequences are listed in the third column of Table 5.

Interestingly, we note that the general formula for the estimate of the jet opening angle

$$\theta_{\rm j} \propto \left(\frac{t_{\rm j,obs}}{1+z}\right)^{(3-s)/(8-2s)} \left(\frac{n_0\eta}{E_{\rm iso}}\right)^{1/(8-2s)}, \quad (24)$$

with $s = 0$ for the homogeneous case and $s = 2$ for the wind case, can be combined with equation (15) to give

$$\theta_{\rm j}\Gamma_0 \propto \left(\frac{t_{\rm j,obs}}{t_{\rm p,obs}}\right)^{(3-s)/(8-2s)}. \quad (25)$$

The product $\theta{\rm j}\Gamma_0$ then depends only on two observables, i.e. the time of the peak of the afterglow $t_{\rm p,obs}$ and the time of the jet break $t_{\rm j,obs}$, and it is independent of the redshift z and the energetic $E_{\rm iso}$ as well as of the density profile normalization n_0 and radiative efficiency η. If also the product $\theta_{\rm j}^2\Gamma_0 =$ const, then we can derive both $\theta_{\rm j} \propto (t_{\rm p,obs}/t_{\rm j,obs})^{(3-s)/(8-2s)}$ and $\Gamma_0 \propto (t_{\rm j,obs}/t_{\rm p,obs})^{(3-s)/(4-s)}$. If the ansatz $\theta_{\rm j}^2\Gamma_0 =$ const will prove to be true, then by simply measuring the peak time and the jet break time of the afterglow light curve we could estimate both $\theta_{\rm j}$ and Γ_0 for any GRB.

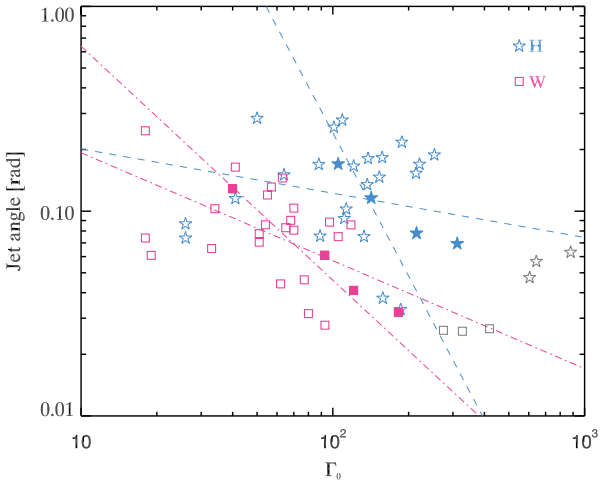

Figure 8. Jet opening angle as a function of Γ_0 for a H (stars) and for a W (squares). Empty symbols show the jet angles estimated by assuming the consistency of our sample with the $E_{\rm peak}$–E_γ relation. Filled symbols refer to the bursts of our sample for which the jet opening angle has been calculated from the measured jet break time of the optical light curves. The two lines (dashed for the H case and dot–dashed for the W case) show the power-law fit of the data points considering $\theta_{\rm jet}$ versus Γ_0 and Γ_0 versus $\theta_{\rm jet}$. The grey symbols show the three long bursts with a peak in the GeV light curve that, if interpreted as afterglow emission, allows us to estimate Γ_0.

In our sample, only for four bursts we can estimate the jet opening angle from the measure of the jet break time of the optical light curve. Their small number does not make possible to directly test the existence of a relation between Γ_0 and $\theta_{\rm j}$. However, an estimate of the jet opening angle can be possible by assuming that all bursts in our sample are consistent with the 'Ghirlanda' relation. Fig. 8 shows the estimated $\theta_{\rm j}$ as a function of Γ_0. Stars (squares) refer to angles derived under the assumption of a H (W). To estimate the jet opening angles we considered the most updated 'Ghirlanda' correlation, which comprises 29 GRBs with measured jet break time (Ghirlanda et al. 2006). For the homogeneous density profile, the relation has the form $\log E_{\rm peak} = -32.81 + 0.70 \log E_\gamma$, while in the case of a W the relation becomes $\log E_{\rm peak} = -50.08 + 1.04 \log E_\gamma$. Given the large scatter of the data points in Fig. 8, we fitted both $\theta_{\rm j}$ versus Γ_0 and Γ_0 versus $\theta_{\rm j}$: we obtain $\theta_{\rm j} \propto \Gamma_0^{-0.22}$ and $\Gamma_0 \propto \theta_{\rm j}^{-2.32}$ for the H case (dashed lines in Fig. 8) and $\theta_{\rm j} \propto \Gamma_0^{-0.52}$ and $\Gamma_0 \propto \theta_{\rm j}^{-1.14}$ for the W case (dot–dashed line in Fig. 8). We conclude that our ansatz $\theta_{\rm j} \propto \Gamma_0^{-1/2}$ is consistent with, but not proven by, this analysis.

An interesting exercise is to estimate the product $\theta_{\rm j}\Gamma_0$. From the observational point of view $\theta_{\rm j}\Gamma \gg 1$ at the end of the prompt phase, so that the decrease of Γ in the afterglow phase, due to the interaction of the GRB fireball with the ISM, gives rise to a jet break when $\theta_{\rm j}\Gamma \sim 1$.

Some numerical simulations (Komissarov et al. 2009) of jet acceleration have shown that a magnetic-dominated jet confined by an external medium should have $\theta_{\rm j}\Gamma_0 \leq 1$. This value is inconsistent with typical values of $\theta_{\rm j}$ and Γ_0: in the case of an homogeneous wind density profile the typical $\theta_{\rm j} \sim 0.1$ radiants (Ghirlanda et al. 2007), while in the case of a wind density profile $\theta_{\rm j} \sim 0.07$ radiants. Combining these values with the average values of Γ_0 estimated in this paper (Table 1) we find $\theta_{\rm j}\Gamma_0 \sim 14$ (5) for the H (W) case.

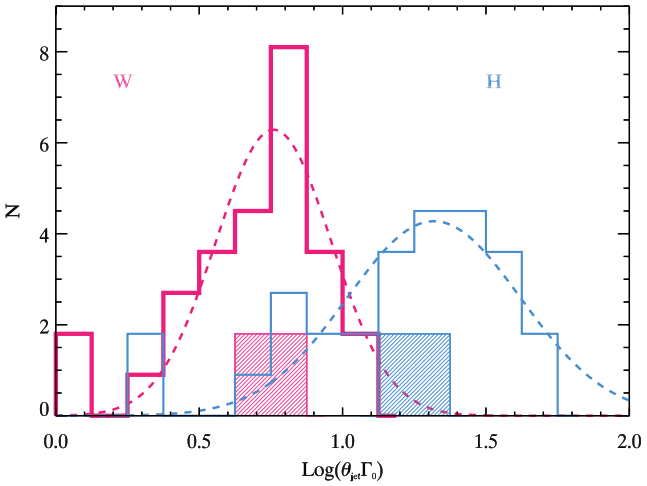

Figure 9. Distribution of $\theta_j\Gamma_0$ in the H and W cases (blue and purple histograms) estimated by assuming the E_{peak}–E_γ relation in the H (Ghirlanda et al. 2004) or W (Nava et al. 2006) cases. The hatched histograms show the few GRBs in our samples for which θ_j has been calculated from the measured jet break time in the optical light curve.

These are approximate values: the sample of GRBs with measured θ_j (Ghirlanda et al. 2007) contains only four bursts of the sample of events of the present paper with estimated Γ_0. However, though somehow speculative, we can derive θ_j for the 32 GRBs of our sample assuming the E_{peak}–E_γ correlation in the H case (Ghirlanda et al. 2004) or in the W (Nava et al. 2006) case. In Fig. 9 we show the distributions of the product $\theta_j\Gamma_0$ in the H case (blue histogram) and in the W case (purple histogram). We note that both are centred around typical values of 20 and 6 (for the H and W cases, respectively). These values are in good agreement with the results of recent simulations of (i) a magnetized jet confined by the stellar material that freely expands when it breaks out the star (Komissarov, Vlahakis & Koenigl 2010) or (ii) a magnetized unconfined split-monopole jet (Tchekhovskoy, McKinney & Narayan 2009; Tchekhovskoy, Narayan & McKinney 2010). A possible test of these two scenarios could be short GRBs where the absence of the progenitor star would prefer model (ii) for the jet acceleration. In our sample only the short/hard GRB 090510 is present. No jet break was observed for this event, and in general we do not yet know if short GRBs follow the same E_{peak}–E_γ correlation of long ones.

ACKNOWLEDGMENTS

We acknowledge ASI (I/088/06/0) and a 2010 PRIN–INAF grant for financial support. We acknowledge the referee for comments and suggestions that improved this work.

REFERENCES

Abdo A. A. et al., 2009a, ApJ, 706, L138
Abdo A. A. et al., 2009b, Nat, 462, 331
Ackermann M. et al., 2010, ApJ, 716, 1178
Amati L. et al., 2002, A&A, 390, 81
Amati L., Frontera F., Guidorzi C., 2009, A&A, 508, 173
Aptekar R. L. et al., 1995, Space Sci. Rev., 71, 265
Band D. L., Preece R., 2005, ApJ, 627, 319
Barniol-Duran R., Kumar P., 2009, MNRAS, 395, 995
Barthelmy S. D. et al., 2005, Space Sci. Rev., 120, 143
Beloborodov A. M., 2002, ApJ, 565, 808
Blandford R. D., McKee C. F., 1976, Phys. Fluids, 19, 1130
Bosnjak Z., Celotti A., Longo F., Barbiellini G., 2008, MNRAS, 384, 599
Butler N. R., Kocevski D., Bloom J. S., Curtis J. L., 2007, ApJ, 671, 656
Butler N. R., Kocevski D., Bloom J. S., 2009, ApJ, 694, 76
Chevalier R., Li W., 1999, ApJ, 520, L29
Costa E. et al., 1997, Nat, 387, 783
Dado S., Dar A., De Rujula A., 2007, ApJ, 663, 400
De Pasquale M. et al., 2010, ApJ, 709, L146
Firmani C. et al., 2005, MNRAS, 360, L1
Frail D. et al., 1997, Nat, 389, 261
Ghirlanda G., Ghisellini G., Lazzati D., 2004, ApJ, 616, 331
Ghirlanda G., Ghisellini G., Firmani C., Celotti A., Bosnjak Z., 2005, MNRAS, 360, 45
Ghirlanda G., Ghisellini G., Firmani C., 2006, New J. Phys., 8, 123
Ghirlanda G., Nava L., Ghisellini G., Firmani C., 2007, A&A, 466, 127
Ghirlanda G., Nava L., Ghisellini G., Firmani C., Cabrera J. I., 2008, MNRAS, 387, 319
Ghirlanda G., Ghisellini G., Nava L., 2010a, A&A, 510, L7
Ghirlanda G., Nava L., Ghisellini G., 2010b, A&A, 511, 43
Ghirlanda G., Ghisellini G., Nava L., Burlon D., 2011, MNRAS, 401, L47
Ghisellini G., Ghirlanda G., Tavecchio F., 2007, MNRAS, 382, L77
Ghisellini G., Nardini M., Ghirlanda G., Celotti A., 2009, MNRAS, 393, 253
Ghisellini G., Ghirlanda G., Nava L., Celotti A., 2010, MNRAS, 403, 926
Gruber D. et al., 2011, A&A, 528, 15
Hascoet R., Vennin V., Daigne F., Mochkovitch R., 2011, preprint (arXiv1101.3889)
Isobe T., Feigelson E. D., Akritas M. G., Babu G. J., 1990, ApJ, 364, 104
Komissarov S. S., Vlahakis N., Koenigl A., Barkov M. V., 2009, MNRAS, 394, 1182
Komissarov S. S., Vlahakis N., Koenigl A., 2010, MNRAS, 407, 17
Krimm H. A. et al., 2009, ApJ, 704, 1405
Liang E.-W., Yi S.-X., Zhang J., 2010, ApJ, 725, 2209
Lithwick Y., Sari R., 2001, ApJ, 555, 540
Lv J., Zou Y.-C., Lei W.-H., 2011, preprint (arXiv:1109.3757)
Meegan C. et al., 2009, ApJ, 702, 791
Molinari E. et al., 2007, A&A, 469, L13
Nakar E., Piran T., 2005, MNRAS, 360, L73
Nava L., Ghisellini G., Ghirlanda G., Tavecchio F., Firmani C., 2006, A&A, 450, 471
Nava L., Ghirlanda G., Ghisellini G., Firmani C., 2008, MNRAS, 391, 639
Panaitescu A., Kumar P., 2000, ApJ, 543, 66
Piran T., Nakar E., 2010, ApJ, 718, L63
Sari R., 1997, ApJ, 489, L37
Sari R., Piran T., 1999, ApJ, 520, L17
Shahmoradi A., Nemiroff R. J., 2011, MNRAS, 411, 1843
Tchekhovskoy A., McKinney J. C., Narayan R., 2009, ApJ, 699, 1789
Tchekhovskoy A., Narayan R., McKinney J. C., 2010, New Astron., 15, 749
Wijers R. A. M. J., Galama T. J., 1999, ApJ, 523, 177
Yonetoku D. et al., 2004, ApJ, 609, 935
Zhao X.-H., Li Z., Bai J.-M., 2011, ApJ, 726, 89
Zou Y.-C., Piran T., 2010, MNRAS, 402, 1854
Zou Y.-C., Fan Y.-Z., Piran T., 2011, ApJ, 726, L2

This paper has been typeset from a TEX/LATEX file prepared by the author.